Journal of The Electrochemical Society

Quantification of the Voltage Losses in the Minimal Architecture Zinc-Bromine Battery Using GITT and EIS

Quantification of the Voltage Losses in the Minimal Architecture Zinc-Bromine Battery Using GITT and EIS

Kevin W. Knehr,[a,b,*] Shaurjo Biswas,[a,b] and Daniel A. Steingart[a,b,c,*,z]

[a]*Department of Mechanical and Aerospace Engineering, Princeton University, Princeton, New Jersey 08544, USA*
[b]*The Andlinger Center for Energy and the Environment, Princeton University, Princeton, New Jersey 08544, USA*
[c]*Department of Chemical and Biological Engineering, Princeton University, Princeton, New Jersey 08544, USA*

The sources of voltage loss in the minimal architecture zinc bromine battery are characterized using the galvanostatic intermittent titration technique (GITT) and electrochemical impedance spectroscopy (EIS) on a cell with a three electrode setup. Monitoring of the electrode voltages during charge/discharge indicate the full cell capacity is limited by the Zn/Zn^{2+} negative electrode. From GITT, the losses in voltage due to mass transport are shown to be relatively small in comparison to the IR resistance in the cell. In addition, it is shown that decreases in the open circuit voltage with respect to theory are likely caused by the complexation of Br_2 into Br_X^-. Using EIS, the charge transfer resistances at each electrode and ohmic resistances of each component are determined. Overall, the main factors restricting the voltage of the cell are the ohmic resistances in the carbon cloth current collectors and in the electrolyte. Additionally, significant charge transfer resistances are observed at the negative electrode near the start of charge and end of discharge, when the amount of zinc plated on the carbon cloth electrode is minimal.

Manuscript submitted August 11, 2017; revised manuscript received September 25, 2017. Published October 12, 2017. This was Paper 20 presented at the National Harbor, Maryland Meeting of the Society, October 1–5, 2017.

The major design criteria for electrochemical energy storage on the grid-scale are low cost and long lifetime. To accomplish this, research efforts have largely focused on the development of low-cost active materials which are incorporated into traditional battery designs.[1–10] These designs typically contain a considerable amount of passive components that are necessary for extending the lifetime of the battery. An undesired consequence of combining inexpensive materials with passive components is the balance-of-plant cost far outweighs the active material cost.

For example, zinc-bromine redox flow batteries have been shown to perform with less than 20% capacity fade for 2,500 cycles.[11,12] However, the cost of this technology (>$200 kWh) is still prohibitive even though the active materials and carbon electrodes only account for ~$8 kWh.[13] The majority of the cost comes from the system level, where complexing agents, separation membranes, and flow systems are used to prevent the corrosive bromine from reacting with the zinc electrode.[14–23]

In light of this fact, our lab has recently developed a minimal architecture zinc-bromine battery (MA-ZBB), which utilizes the same chemistry from commercial zinc-bromine flow batteries, but does not require the need of any passive components, significantly reducing the cost (projected ~$94/kWh).[24] The MA-ZBB is composed of two carbon based electrodes, which are spatially separated in the vertical direction, in an aqueous electrolyte containing zinc-bromide salt. The battery does not contain any passive components for controlling bromine/zinc interaction (i.e. pumps, membranes or complexing agents). Instead, the electrodes are vertically separated to utilize the variations in density between bromine and the aqueous electrolyte as an advantage to minimize self-discharge. At the negative electrode on top of the cell, zinc ions are reduced (Zn) and oxidized (Zn^{2+}) on a carbon cloth during charge and discharge, respectively.

$$Zn \underset{charge}{\overset{discharge}{\rightleftharpoons}} Zn^{2+} + 2e^- \quad [1]$$

At the positive electrode, which is located on the bottom of the cell, bromide ions are oxidized (Br_2) and reduced (Br^-) within a carbon foam electrode (CFE).

$$Br_2 + 2e^- \underset{charge}{\overset{discharge}{\rightleftharpoons}} 2Br^- \quad [2]$$

To date, a lab-scale cell has demonstrated an energy efficiency of >60% and a coloumbic efficiency of >90% for over 1000 cycles at an energy density of ~10 Wh/L.[24] Further improvements in the performance are required to increase the viability of this technology for grid-level energy storage. In particular, the energy efficiency of 60% signifies considerable voltage losses in the system, which reduce the energy density and increase the overall cost. In this work, we seek to quantify these sources of voltage loss to identify viable methods for improving the energy efficiency of the MA-ZBB. As an added bonus, this study provides baseline performance metrics for a no-flow zinc/bromine battery. To accomplish this, we use the galvanostatic intermittent titration technique (GITT) and electrochemical impedance spectroscopy (EIS). Experiments are carried out on a lab-scale cell which includes a silver|silver chloride reference electrode for determining the contributions of the positive and negative electrodes toward the overall losses in the cell.

Experimental

Electrode fabrication.—The carbon foam electrode (CFE) used as the positive electrode was fabricated using a method similar to our previous work.[24] In short, the electrode was composed of 90% carbon and 10% polyvinylidene fluoride (PVDF) by weight. The carbon was 50:50 carbon black (EC600JD, AkzoNobel) and graphite (496596-113.4G, Aldrich) by weight. The electrodes were fabricated by combining the carbon with a solution of 5% PVDF and 95% N-Methyl-2-pyrrolidone (by weight) and compressing the resulting slurry using a custom built mold. During compression, a thin sheet of carbon cloth (CCP, Fuel Cell Earth) was inserted into the CFE to act as a current collector lead. The CFE was cured in a vacuum oven at 130°C for 8 hours.

Cell construction.—A picture of the cell used in the experiments is shown in Figure 1. The cell contains the CFE at the bottom of the electrode which is connected to the outside by a carbon cloth lead, which is 1.2 cm wide and 6.2 cm long. The carbon cloth lead is sealed by applying a dispersion of polytetrafluoroethylene (PTFE) in water to the cloth, evaporating the water over a hot plate, and wrapping

*Electrochemical Society Member.
[z]E-mail: steingart@princeton.edu

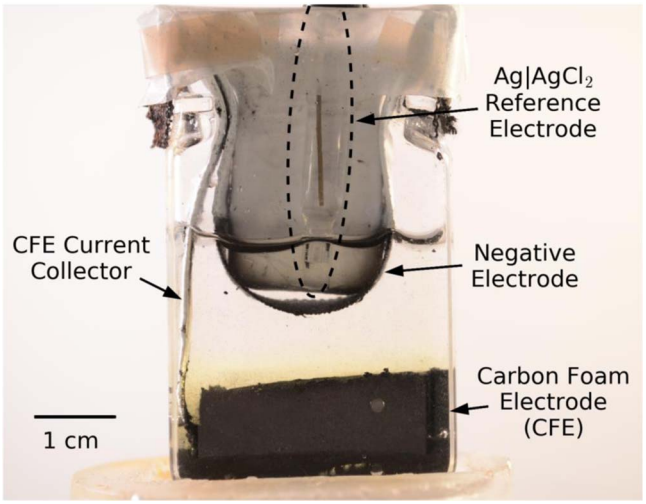

Figure 1. Image of the MA-ZBB lab-scale cell in the discharged state.

the lead in PTFE tape. The same carbon cloth material (sealed in the same manner) is used as the substrate and electrical lead at the top of the cell for the zinc plating and stripping reaction at the negative electrode. The active area is 4.5 cm^2 and the current collector lead out of the cell is 1.2 cm wide and 2.5 cm long. The shape of the negative electrode cloth is maintained using a 3D printed component (Form 1+) wrapped in PTFE tape and heat sealed. A $Ag|AgCl_2$ reference electrode in 3 M NaCl is placed above the negative electrode, which acts as a protective barrier to prevent any Br_2 generated in the cell from reaching the reference electrode (i.e., the Zn on the negative electrode will react with any Br_2 diffusing toward the top of the cell). All tests were performed with 15 mL of 1.86 M $ZnBr_2$ aqueous solution.

Electrochemical testing.—Electrochemical tests were performed using a μAutolabIII potentiostat (Metrohom, USA). Galvanostatic intermittent titration technique (GITT) was performed at four different rates on the same cell (5, 10, 15, and 20 mA). Prior to GITT, the cell was cycled four times at the specified rate. Each cycle consisted of a 4 hour charge, a 10 minute rest, and a discharge to a cutoff voltage of 1.1 V. The 4 hour charge/discharge time was chosen to represent a renewable integration application.[25]

After the break-in cycles, GITT was performed by alternating between 30 minutes of applied current and 10 minutes of rest. Eight measurements were taken during charge, corresponding to 4 hours of total charge time. During discharge, measurements were taken until the 1.1 V cutoff was reached during an applied current step. GITT experiments were performed with the potentiostat in a two-electrode configuration (i.e., voltage and current were only monitored between the positive and negative electrodes). The voltage differences between i) the negative electrode and reference electrode and ii) the negative electrode and positive electrode were monitored simultaneously every 50 ms using a Particle Core microcontroller. The voltage of the $Ag|AgCl_2$ reference electrode was measured against another $Ag|AgCl_2$ reference electrode before and after each GITT experiment to determine the electrode drift due to diffusion of ions across the frit. A linear correction was applied to all voltage values based on the drift.

Following the full round of GITT, electrochemical impedance spectroscopy (EIS) experiments were performed using the μAutolabIII potentiostat. For all EIS experiments, the cell was charged at 20 mA for 30 minutes, rested for 5 minutes, and charged at 1 mA for 12 minutes to equilibrate the voltage. Next, EIS was conducted galvanostatically at 1 ± 0.9 mA with a frequency range from 100 kHz to 10 mHz. The sinusoidal perturbation represents the smallest value capable of producing a sizeable enough voltage change in our system to generate a repeatable impedance measurement. This procedure was completed 8 times during charging, corresponding to 4 hours of total charge time. The same procedure was then repeated during discharge (with the current direction reversed). The EIS experiments were first run with the potentiostat in the three electrode configuration, using the negative electrode as the working electrode. Next, the same tests were run using the positive electrode as the working electrode. All data was analyzed using Python.

Results and Discussion

Voltage curves during charge/discharge cycles at four rates are shown in Figure 2 for the full cell (Fig. 2a), the negative electrode (Fig. 2b), and the positive electrode (Fig. 2c). All data was taken from the fourth cycle at a given rate. The voltage at the positive electrode was obtained by adding the full cell voltage to the negative electrode voltage, which were obtained simultaneously using the microcontroller. The coulombic efficiencies at 5, 10, 15, and 20 mA are 83.5%, 90.0%, 90.9%, and 92.5%, respectively. The energy efficiencies are 77.4%, 78.1%, 74.5%, and 71.4% at the same rates, respectively. The standard error for the coulombic and energy efficiency during cycling of the experimental cell are ±1.4% and ±1.0%, respectively.

According to the data, for all rates, the discharge capacity of the cell is limited by the amount of zinc at the negative electrode, as indicated by the corresponding spikes in voltage between the full cell (2a) and the negative electrode (2b) toward the end of each cycle. The negative electrode could be limiting capacity for two reasons: i) hydrogen evolution during charging limits the total amount of plated zinc and ii) the self-discharge reaction between bromine and zinc is detaching zinc dendrites. The detaching of dendrites is required because simple self-discharge would produce equal losses in the bromine and zinc capacity, which would produce spikes in voltage at both electrodes toward the end of discharge. A more in-depth quantification of these two mechanisms is currently out of the scope of this work.

In terms of voltage loss, Fig. 2c indicates that the positive electrode has much higher resistive losses because its voltage changes significantly with applied current, especially when compared to the negative electrode. To better quantify the voltage losses, the galvanostatic intermittent titration technique was applied to the cell at each rate.

Galvanostatic intermittent titration technique (GITT).—The voltage recovery data obtained from GITT while cycling the cell are shown in Figure 3. The voltage recovery is defined as the change in voltage with respect to the voltage immediately before the current was interrupted. All times are reported with respect to when the current was interrupted. Figures 3a and 3b show the voltage recovery of the full cell during charging and discharging, respectively. In Fig. 3a, the arrows indicate an increase in capacity from green to red. In Fig. 3b, the arrows indicate an increase in depth of discharge from green to red.

Interpretation of the data can be broken into two parts. First, the initial, abrupt change in voltage over the first 50 ms corresponds to ohmic and charge transfer resistances. The resistance associated with this jump is referred to as IR resistance since the voltage penalty associated with these resistances should scale roughly linearly with current. Second, the continual voltage recovery over the next 10 minutes corresponds to mass transfer of species impacting the open circuit voltage.

The IR resistances during charging and discharging for all cases can be found in Figure 4. The inclusion of the reference electrode in the cell made it possible to resolve the full IR resistance into positive electrode and negative electrode components. According to the figure, the positive electrode (Br^-/Br_2) is responsible for the majority of the IR resistance. At all states of charge, over two-thirds of the IR resistance can be attributed to the ohmic and charge transfer resistances measured at that electrode. At low states of charge toward the end of discharge, the IR resistance is shown to increase, which is caused by increases in the resistance at the negative electrode. This can likely be

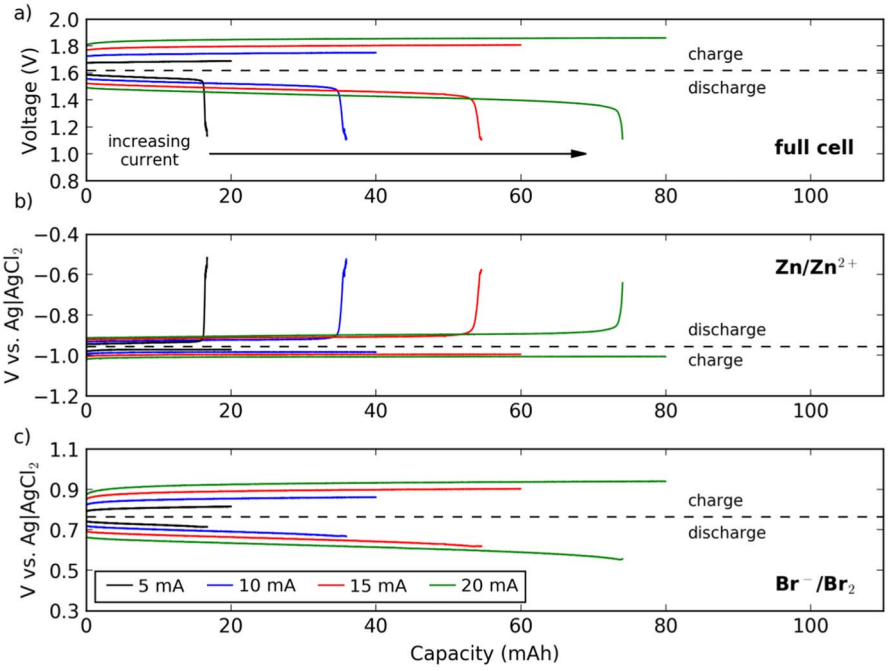

Figure 2. Voltage curves during charge/discharge of the lab-scale cell at four different currents, whereby the cell was charged for four hours and then discharge to a 1.1 V cutoff. Graphs show the measured voltage between a) the positive and negative electrodes; b) the negative electrode and the reference electrode; and c) the positive electrode and the reference electrode. All curves were taken from the fourth cycle at the specified current.

contributed to decreases in available zinc at the negative electrode. A more in depth quantification of these losses is obtained from EIS in the next section.

Figure 5 quantifies the voltage recovery after the initial IR jump. This data describes the voltage losses associated with mass transport in the system. During charge (Fig. 5a), depleted Zn^{2+} at the negative electrode|electrolyte interface and excess Br_2 and depleted Br^- at the positive electrode|electrolyte interface increase the voltage difference between the electrodes. During discharge (Fig. 5b), excess Zn^{2+}, depleted Br_2 and excess Br^- lower the voltage. The figure shows the combined, full cell mass transport voltage losses. The positive and negative electrode components could not be resolved because the junction

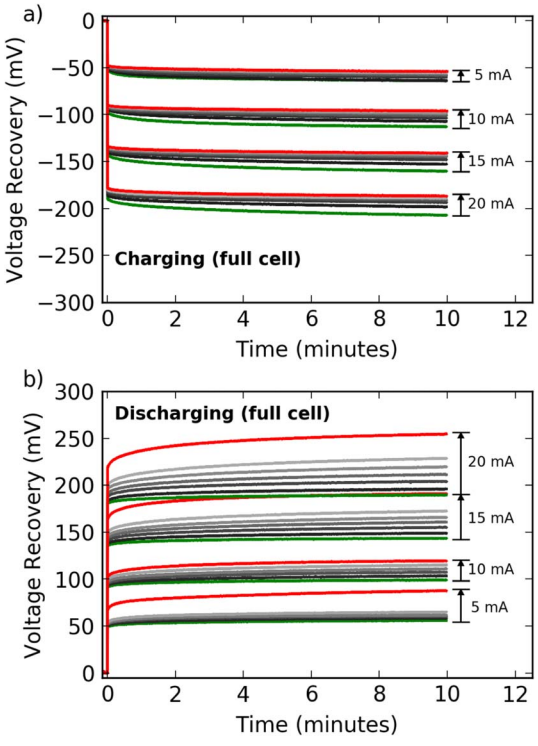

Figure 3. Voltage recovery upon interruption of current during a) charging and b) discharging. Time is reported with respect to the start of current interruption. Arrows in a) correspond to increased charging, where the green and red lines refer to the voltage recovery after charging 0.5 and 4 hours, respectively. Arrows in b) correspond to increased depths of discharge, where green lines refer to voltage recovery after discharging 0.5 hrs and every subsequent line is an additional half hour.

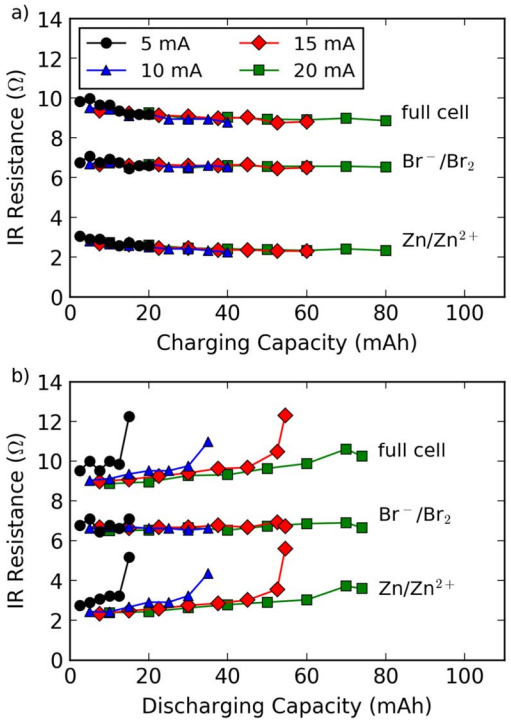

Figure 4. Compilation of the IR resistances obtained from the GITT experiments at each current rate during a) charging and b) discharging. At all rates, the cell was charged for a total of four hours followed by a discharge to 1.1 V with GITT measurements taken every 30 minutes. IR resistances were calculated by dividing the initial voltage jump by the applied current.

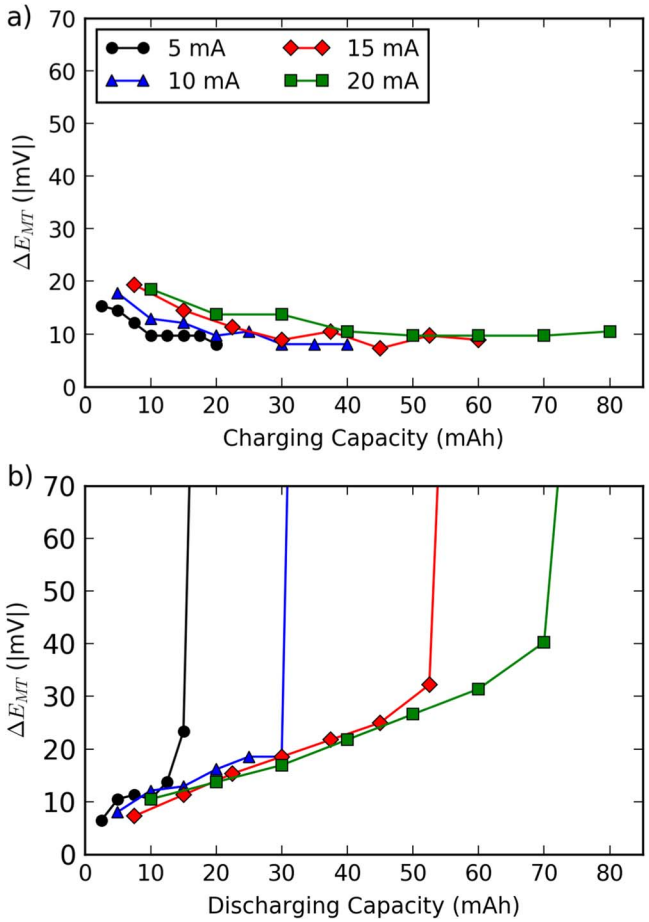

Figure 5. Total voltage recovery during the 10 minutes after the initial IR jump during a) charging and b) discharging. Values provide an indication of voltage loss due to poor mass transport.

potential across the frit of the reference electrode was impacted by the local Zn^{2+} concentration at the negative electrode, yielding constant potential differences between the reference and negative electrodes during the mass transport portion of the voltage recovery.

During charging, the mass transport voltage losses increase with increasing rates, but remain below 20 mV for all rates and at all capacities. During discharging, the voltage losses are more similar with rate, but increase substantially with increased depth of discharge (higher capacity). The increased voltage losses can be attributed to the low concentration of Br_2 in the cell (see Figure 7), which causes poor diffusion to the positive electrode surface. A similar voltage loss is not observed during charging because the reactants during charging, Br^- and Zn^{2+}, are in excess in the system, resulting in easier diffusion to the electrode surfaces. At the end of discharge, for all rates, the mass transport losses increase substantially as Br_2 and Zn become depleted.

In addition to studying voltage loss, GITT can be used to probe the thermodynamic state of the battery during charge/discharge. For instance, the voltage curves in Figure 3 all plateau to a steady state value after ~10 minutes. This plateau voltage represents the thermodynamic/open-circuit voltage of the cell. These voltages are represented as data points in Figure 6. Slight variations in the open circuit voltage at each rate can likely be attributed to different amounts of excess bromine in the cell. Excess bromine was likely present because the GITT measurements were conducted on the fourth cycle and all cycles had <93% coulombic efficiency. The theoretical open circuit voltage (OCV) can be calculated using the Nernst equation, as

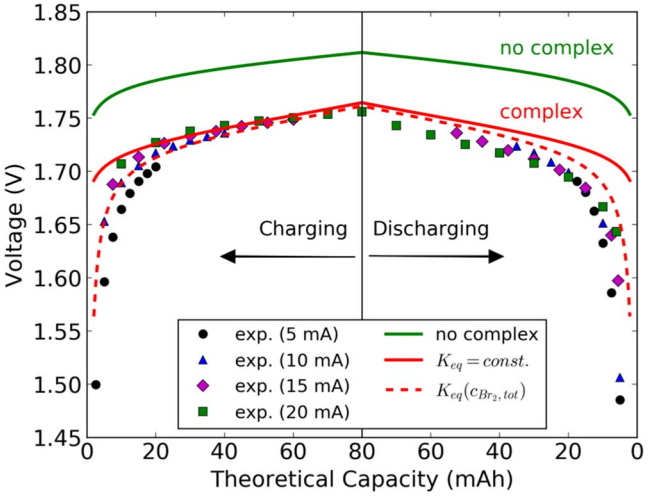

Figure 6. Open circuit voltage of the minimal architecture zinc bromine battery obtained from GITT while cycled at a) 5, b) 10, c) 15, and d) 20 mA.

follows:

$$U = U_0 + \frac{RT}{2F} ln\left(\frac{c_{Br_2}}{c_{Br^-}^2 c_{Zn^{2+}}}\right) \quad [3]$$

where U_0 is the standard reference potential between the positive and negative electrodes (1.849 V),[26] R is the ideal gas constant, T is the temperature, and F is Faraday's constant. The terms inside the logarithm represent the concentrations of aqueous phase bromine, bromide ions, and zinc ions, respectively.

At first, to calculate U, it was assumed that all bromine produced during charging went into the electrolyte as Br_2(aq). Self-discharge was ignored. In addition, bromine diffusion out of the CFE was assumed to be negligible. This assumption arose from the fact that the relaxation time corresponding to complete bromine diffusion within the cell, determined from L^2/D, was estimated to be ~50 hours. L is the average distance between the electrodes (1.5 cm) and D is the diffusion coefficient of Br_2 (1.31×10^{-5} cm^2 s^{-1}).[26] This relaxation time is much larger than the 10 minute voltage recovery observed experimentally, suggesting the voltage recovery over short times can mainly be attributed to relaxation of Br_2 within the pores of the CFE. A similar analysis was done on the Zn^{2+} ions to justify the final assumption that the zinc ions within the CFE had no impact on the total concentration.

Based on these assumptions, the concentration of each species at each time was determined using the following ordinary differential equation:

$$\frac{dc_i}{dt} = \frac{s_i I}{n_i F V_i} \quad [4]$$

where s_i is the stoichiometric factor of species 'i', n_i is the number of equivalent electrons per mole of species, and I is the reaction rate in amps (positive for oxidation, negative for reduction). An overview of the values can be found in Table I. In the table, c_0 is the initial concentration of $ZnBr_2$, V_{cell} is the total electrolyte volume, V_{CFE} is the total CFE volume (5.5 mL), and ε is the porosity of the CFE (45%).[24]

Table I. Parameters and initial conditions used to calculate the concentration in the cell for the open circuit voltage approximation.

Species	s_i	n_i	V_i (dm^3)	$c_i(0)$ (M)
Zn^{2+}	1	2	V_{cell} - εV_{CFE}	c_0
Br^-	2	2	εV_{CFE}	$2c_0$
Br_2	1	2	εV_{CFE}	0

The results of the calculation are shown as the solid green line in Figure 6. At all rates, Eq. 4 significantly overestimates the experimental open circuit voltage by 50 to 300 mV. An overestimation of this size can only occur if the concentration term within the natural logarithm in Eq. 3 is several orders of magnitude lower than predicted, suggesting the concentration of at least one species is much lower. One possibility is that Br_2 could be intercalating into the graphite in the CFE; however, this is highly unlikely because the electrochemical intercalation of Br_2 into graphite only occurs at very high overpotentials and very high reaction rates, which drive the local concentration of Br_2 near the graphite surface to extremely high values.[27,28] These conditions are not met in our high surface area CFE. The most likely cause is the complexation of Br_2(aq) into polyhalide Br_X^-(aq) (where X = 3, 5, 7, etc.).[18,29,30]

The complexed Br_2 was accounted for by assuming Br_3^- was the only complex. The bromine species were assumed to be in equilibrium because the relaxation time of the equilibrium reaction is on the order of nanoseconds.[30] At first, it was assumed the value of the equilibrium constant did not change with depth of charge/discharge. Equation 4 was still used to calculate the Zn^{2+} concentration. The concentrations of the bromine species were calculated using the following set of equations:

$$\frac{dc_{Br_{2,tot}}}{dt} = \frac{I}{2F\varepsilon V_{CFE}} \quad [5]$$

$$c_{Br_{2,tot}} = c_{Br_2} + c_{Br_3^-} \quad [6]$$

$$2c_0 = c_{Br^-} + 2c_{Br_2} + 3c_{Br_3^-} \quad [7]$$

$$K_{eq} = \frac{c_{Br_3^-}}{c_{Br^-}c_{Br_2}} \quad [8]$$

Note that higher order complexes likely exist in solution and could be included in the model by expanding Equations 6 and 7 and including an equilibrium equation for each additional species, which would resemble Equation 8. These species were not included in the present model to minimize the amount of fitted parameters to a single equilibrium constant (K_{eq}).

The results of the open circuit voltage calculation with complexed Br_2 are shown as solid, red lines in Figure 6. K_{eq} was set equal to 35 M^{-1} in order to provide a best fit with the data at all rates. This value is similar to the equilibrium constant of Br_2 in pure water, where reported values have ranged from 17 to 50 M^{-1}.[29,30] At high capacities, where bromine is at higher concentrations, Equations 3–8 produce a very good fit to the experimental data. At low capacities, where Br_2 concentrations are expected to be low, the new set of equations still overestimates the open circuit potential.

An explanation for this discrepancy could be that the equilibrium constant of the bromine complexes also depends on the local concentrations of the bromine species. This would suggest that Br_2 is more likely to form complexes at low concentrations in the electrolyte. To test this hypothesis, we altered the equilibrium constant using the following empirical equation:

$$K_{eq} = K_1 exp\left(\frac{K_2}{c_{Br_{2,tot}}}\right) \quad [9]$$

The dashed, red line in Figure 6 represents the results of the open circuit voltage calculations using Equations 4 to 9, where K_1 and K_2 in Eq. 9 are equal to 35 M^{-1} and 0.15 M, respectively. This expression yields good agreement with experimental data at all rates, further indicating that Br_2 exists as polyhalides in solution. Note that simulations of the open circuit voltage were also conducted using Equations 3–8 (with a constant K_{eq}) and adding an additional equilibrium equation to account for the formation of Br_5^- based on the following mechanism:

$$Br_2 + Br_3^- \rightleftharpoons Br_5^- \quad [10]$$

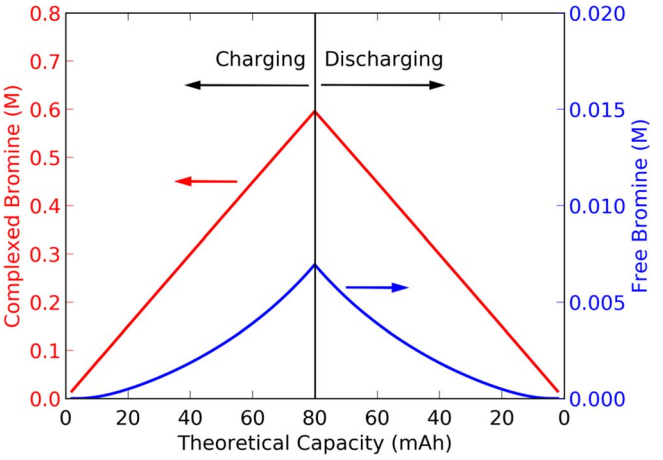

Figure 7. Concentration of a) free and b) complexed bromine in the CFE as calculated from Equations 4 to 9. Data in the figure was used to produce the dashed, red line in Figure 6.

Inclusion of this species did not improve agreement in the open circuit voltage for a wide range of equilibrium constants. Therefore, the result was not included in the figure.

The results in Figure 6 indicate most of the Br_2 exists in a complexed form. For instance, Figure 7 provides the calculated concentrations of a) free and b) complexed Br_2(aq) that were used to generate the dashed, red lines in Figure 6. This data provides a reasonable estimate of the orders of magnitude of the concentrations of bromine species needed to fit the experimental open circuit voltage data. The results suggest that the amount of complexed Br_2 in the electrolyte is over 60× higher than free Br_2. This negatively impacts the energy density of the cell by lowering the open circuit voltage at all states of charge.

Note that the data in Figure 7 was calculated assuming only Br_3^- was present; however, higher order species (Br_5^-, Br_7^-, etc.) likely exist. Addition of these species would increase the complexity of the present model without changing the general conclusion that complexing Br_2 is negatively impacting the open circuit voltage. For future models, inclusion of these higher order species may be important, especially in studies seeking to characterize the reaction kinetics since the relative proportion of the bromine species (and the rates of dissociation back into Br_2) likely have a strong impact on the kinetics of the reduction reaction.

Electrochemical impedance spectroscopy (EIS).—Electrochemical impedance spectroscopy was run on the cell to better understand the causes of the IR resistance at each electrode obtained during GITT. The resulting Nyquist plots are shown in Figure 8 during a) charging and b) discharging of the cell at a 20 mA rate. In Fig. 8a, the capacities indicate the amount of charge passed during charge, with 10 mAh and 80 mAh corresponding to the beginning and end of charge, respectively. In Fig. 8b, the capacities indicate the amount of charge passed during discharge.

For each set of data in the Nyquist plots, the real impedance value at the start of the semicircle corresponds to the ohmic resistance between the reference and positive/negative electrode. The diameter of the semicircle corresponds to the charge transfer resistance associated with the reactions at the electrode. Obvious trends are observed in the resistances at both electrodes during charging and discharging.

To more accurately quantify these trends, the semi-circular region of the EIS data was fit to a Randles equivalent circuit.[31] The diffusive portion at low frequencies are ignored in the fit because the objective of this experiment is to quantify the ohmic and charge transfer resistances in the cell. A schematic of the circuit and the resistances obtained from the fit at each electrode are shown in Figure 9a. The fitted curves are also shown overlaid on top of the experimental data in Figure 8. At the

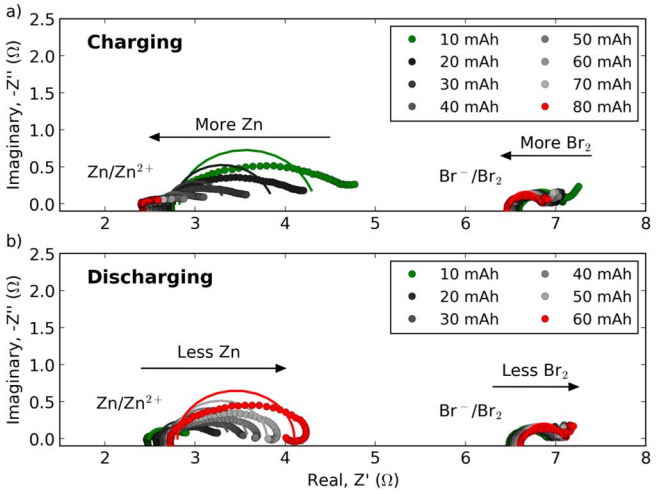

Figure 8. Nyquist plots from electrochemical impedance spectroscopy taken at various capacities during a) charging and b) discharging at a 20 mA rate. Green and red datasets correspond to start and end of charge/discharge, respectively. Circles are experimental data while lines are fits of semi-circular region to Randles circuit (see Figure 9 for description).

positive electrode, slight deviations between the fit and experimental data can be attributed to the simplification of the Randles circuit, which does not account for variations in reaction distribution and related ionic resistances associated with the thick CFE. At the negative electrode, deviations can be attributed to the influence of the hydrogen evolution reaction. Even with these deviations, conclusions about the relative importance of the resistances at each electrode remain valid. The results indicate that the ohmic resistances in the cell are more problematic than the charge transfer resistance. For instance, the black diamonds in the figure indicate that the resistance associated with the Br_2/Br^- reaction ($R_{CT,pos}$) is less than 0.5 Ω during the entire cycle. The low $R_{CT,pos}$ can be attributed to the high surface area of the CFE.

In addition, the red squares indicate that, except at low states of charge (start of charge and end of discharge), the charge transfer resistance associated with the Zn/Zn^{2+} reaction ($R_{CT,neg}$) is much lower than the ohmic resistances in the cell. The relatively high $R_{CT,neg}$ at the low states of charge are attributed to a lack of zinc on the carbon cloth electrodes. This is especially noticeable at the end of discharge where $R_{CT,neg}$ rapidly increases due to a lack of zinc for oxidation. The amount of zinc on the electrode is likely also responsible for the slight decrease in the ohmic resistance at the negative electrode ($R_{\Omega,neg}$) during higher states of charge (circles in Fig. 9a). For most of the cycle, $R_{\Omega,neg}$ is high relative to R_{CT} due to the ohmic drop associated with the carbon cloth current collector.

The main takeaway from Figure 9a is that the ohmic resistance measured between the positive and reference electrode ($R_{\Omega,pos}$) is the most problematic for cell performance. Referring back to Figure 1, this ohmic resistance is comprised of four parts: i) the electronic resistance of the carbon cloth current collector, ii) the contact resistance between the CFE and current collector, iii) the resistance in the CFE, and iv) the ionic resistance between the electrodes. The deconvolution of the positive electrode resistance into these components is shown in Figure 9b.

To determine the contributions from each component, first, the current collector resistance (R_{CC}) was measured using a Fluke 83 Multimeter. Next, the electrolyte resistance (R_{elec}) was determined using the following equation:

$$R_{elec} = \frac{\rho L}{A} \qquad [11]$$

where L is the average distance between the electrodes (1.5 cm), A is the cross sectional area of the negative electrode (4.5 cm^2), and ρ is the resistivity of the electrolyte obtained from Ref. 20, which

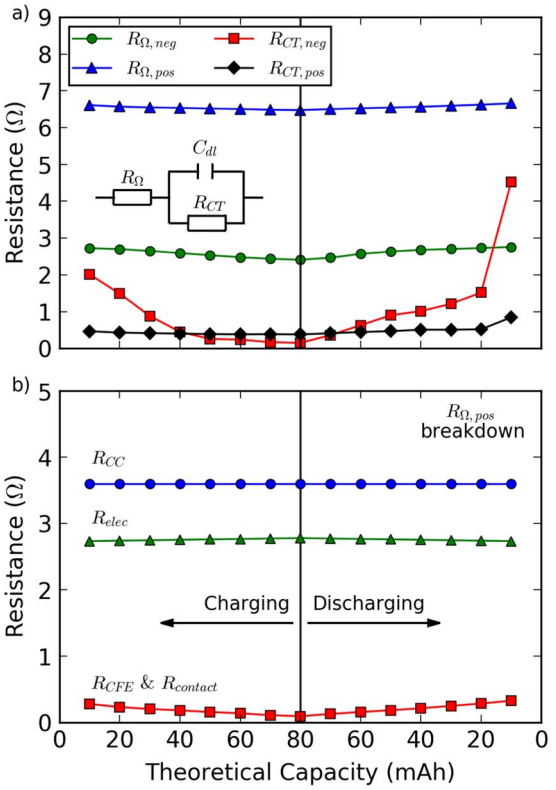

Figure 9. a) Results of fitting Nyquist plots in Figure 8 to a Randles circuit. R_Ω and R_{CT} refer to the ohmic and charge transfer resistance, respectively. b) Breakdown of the ohmic resistance measured between the positive electrode and the reference electrode. R_{CC} is the current collector resistance. R_{elec} is the resistance in the electrolyte between the CFE and the negative electrode. R_{CFE} is the resistance within the CFE. $R_{contact}$ is the contact resistance between the CFE and the current collector.

was adjusted based on variations in the electrolyte concentration. The CFE and contact resistance could not be decoupled, but their combined contribution, which was minimal, was determined as follows:

$$R_{CFE} + R_{contact} = R_{\Omega,pos} - R_{CC} - R_{elec} \qquad [12]$$

The results indicate that the ohmic resistance in the electrolyte and current collector are the major causes of the high positive electrode resistance.

Summary of results.—A summary of the voltage losses in the cell at all four rates during discharge can be found in Figure 10. All the voltage losses were obtained from the GITT and EIS measurements above. The charge transfer and ohmic resistances obtained from the EIS experiments at 20 mA were used to estimate the voltage loss at the other rates. To accomplish this, it was assumed that these resistances were a function of the remaining discharge capacity in the cell, and the values at 5, 10, and 15 mA were interpolated from the 20 mA data. The only resistance where this method could produce noticeable errors is $R_{CT,neg}$, as the morphology of the zinc structure likely depends on charge/discharge rate. However, this method still provides a reasonable estimation of the overall contribution of $R_{CT,neg}$ to the cell loss.

In the figure, the red bars at the bottom represent the voltage loss due to complexing of the Br_2. This was calculated by taking the difference between the theoretical OCV calculated using Equations 3–4 (green lines in Fig. 6) and the experimental OCV (data points in Fig. 6). Unlike the other sources of voltage loss, this value indirectly impacts the energy efficiency because it shifts both the charge and discharge voltage downward. The other sources of voltage loss directly impact the energy efficiency because they increase the separation

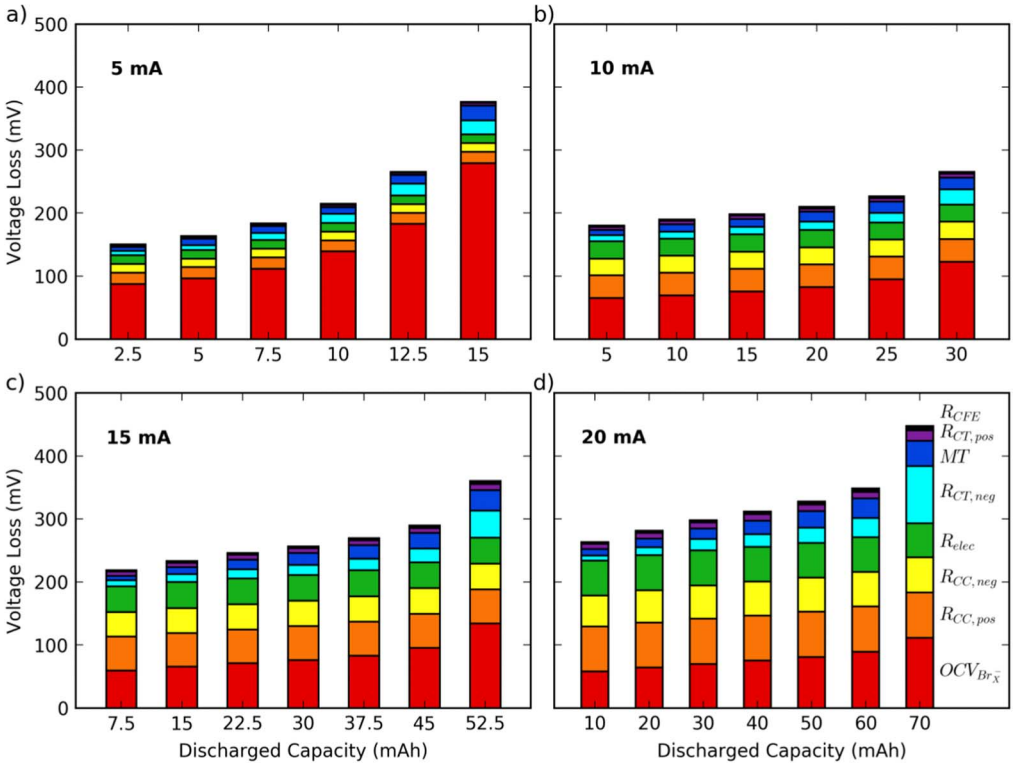

Figure 10. Summary of the voltage losses during discharge obtained from GITT and EIS analysis. Description from bottom to top: i) open circuit voltage (OCV) loss due to bromine complexation, ii) positive current collector resistance, iii) negative current collector resistance, iv) electrolyte resistance, v) negative electrode charge transfer resistance, vi) mass transport voltage loss, vii) positive electrode charge transfer resistance, and viii) resistance in CFE. Ionic resistance in the CFE was the only resistance not included because it could not be determined with the above experiments (see discussion).

between the charge and discharge curves. Among these sources, ohmic resistance in the current collectors and electrolyte - orange, yellow, and green (color online) - are the main factors reducing the efficiency of the cell. Combined, these three factors account for 47 to 72%, 64 to 78%, 60 to 84%, and 54 to 86% of the resistive voltage loss (OCV losses not included) during discharge at 5, 10, 15, and 20 mA, respectively. The only other major factor is the charge transfer resistance in the negative electrode near the end of discharge when there is minimal zinc on the carbon cloth electrode. In addition to the values reported herein, there is an electrolyte resistance within the CFE that could not be determined from the above experiments. The total contribution of this resistance to the voltage loss will depend on the reaction distribution within the CFE, which can be accurately determined with numerical simulations using porous electrode theory. This additional resistance will increase the voltage loss due to ohmic resistance, further reinforcing the conclusion that ohmic losses are one of the main issues in the cell.

Conclusions

The voltage loss in the minimal architecture zinc-bromine battery mainly arises from the ohmic resistances in the carbon cloth current collectors and within the electrolyte between the electrodes. Mass transport resistance associated with diffusion of the active species away from the electrode surface and charge transfer resistance associated with the reactions are not major causes of voltage loss for most of the discharge process. One exception is at low states of charge (start of charge and end of discharge) where the charge transfer resistance at the negative electrode has a similar magnitude to the ohmic resistances due to a lack of zinc metal on the carbon cloth electrode.

In addition, the open circuit voltage of the cell was shown to decrease at all states of charge due to the complexing of Br_2 into Br_X^-. This complexing negatively impacts the energy density of the cell. It was suggested that a larger fraction of Br_2 was complexed at lower total concentrations of Br_2 in the cell.

Acknowledgments

This work was supported by Israel Chemicals Ltd (ICL). The authors graciously thank Hang Huynh for her time.

ORCID

Shaurjo Biswas https://orcid.org/0000-0001-8958-2673
Daniel A. Steingart https://orcid.org/0000-0002-8184-9641

References

1. Z. Yang et al., *Chem. Rev.*, **111**, 3577 (2011).
2. B. Dunn, H. Kamath, and J.-M. Tarascon, *Science*, **334**, 928 (2011).
3. M. Skyllas-Kazacos, M. H. Chakrabarti, S. A. Hajimolana, F. S. Mjalli, and M. Saleem, *J. Electrochem. Soc.*, **158**, R55 (2011).
4. Y. Ito et al., *J. Power Sources*, **196**, 2340 (2011).
5. Y. Lu, L. Wang, J. Cheng, and J. B. Goodenough, *Chem. Commun.*, , **48**, 6544 (2012).
6. J. F. Whitacre et al., *J. Power Sources*, **213**, 255 (2012).
7. M. D. Slater, D. Kim, E. Lee, and C. S. Johnson, *Adv. Funct. Mater.*, **23**, 947 (2013).
8. B. Huskinson et al., *Nature*, **505**, 195 (2014).
9. T. Ouchi, H. Kim, X. Ning, and D. R. Sadoway, *J. Electrochem. Soc.*, **161**, A1898 (2014).
10. T. Gupta et al., *J. Power Sources*, **305**, 22 (2016).
11. P. Lex and B. Jonshagen, *Power Engineering Journal*, **13**, 142 (1999).
12. H. Chen et al., *Prog. Nat. Sci.*, **19**, 291 (2009).
13. R. M. Darling, K. G. Gallagher, J. A. Kowalski, S. Ha, and F. R. Brushett, *Energy Environ. Sci.*, **7**, 3459 (2014).
14. K. J. Cathro, K. Cedzynska, D. C. Constable, and P. M. Hoobin, *J. Power Sources*, **18**, 349 (1986).
15. K. Cedzynska, *Electrochim. Acta*, **40**, 971 (1995).
16. J. D. Jeon, H. S. Yang, J. Shim, H. S. Kim, and J. H. Yang, *Electrochim. Acta*, **127**, 397 (2014).
17. M. Mastragostino and S. Valcher, *Electrochim. Acta*, **28**, 501 (1983).
18. D. J. Eustace, *J. Electrochem. Soc.*, **28** (1979).

19. Q. Lai, H. Zhang, X. Li, L. Zhang, and Y. Cheng, *J. Power Sources*, **235**, 1 (2013).
20. H. S. Lim, A. M. Lackner, and R. C. Knechtli, *J. Electrochem. Soc.*, **124**, 1154 (1977).
21. J. H. Yang, H. S. Yang, H. W. Ra, J. Shim, and J. -D. Jeon, *J. Power Sources*, **275**, 294 (2015).
22. L. Zhang, H. Zhang, Q. Lai, X. Li, and Y. Cheng, *J. Power Sources*, **227**, 41 (2013).
23. P. Leung et al., *RSC Adv.*, **2**, 10125 (2012).
24. S. Biswas et al., *Energy Environ. Sci.*, **10**, 114 (2017).
25. *Electricity Energy Storage Technology Options: A White Paper Primer on Applications, Costs, and Benefits*, EPRI, Palo Alto, CA, (2010).
26. T. I. Evans and R. E. White, *Electrochim. Acta*, **23**, 1351 (1978).
27. J. R. Gaier, N. F. Ditmars, and A. R. Dillon, *Carbon*, **43**, 189 (2005).
28. C. T. Ho and D. D. L. Chung, *Carbon*, **28**, 521 (1990).
29. M. Eigen and K. Kustin, *J. Am. Chem. Soc.*, **84**, 1355 (1962).
30. M. F. Ruasse, J. Aubard, B. Galland, and A. Adenier, *J. Phys. Chem.*, **90**, 4382 (1986).
31. C. N. Sun et al., *ECS Electrochemistry Letters*, **2**, A43 (2013).